BJRS

BRAZILIAN JOURNAL
OF
RADIATION SCIENCES
11-01A (2023) | 01-20 | e2193

Computational analysis for wax detection in deepwater pipelines using nuclear techniques

Leite[a], N. M.; Lira[a], C. A. B. O.; Rodriguez[b], A. G.

[a] *Northeast Regional Nuclear Science Center, Av. Prof. Luiz Freire, 200 - University City - CEP 50.740-540, Recife, Pernambuco, Brazil*

[b] *Federal University of Pernambuco/Department of Nuclear Energy, Av. Prof. Luiz Freire, 1000 - University City - CEP 50.740-545, Recife, Pernambuco, Brazil*

nalber.leite@cnen.gov.br

carlos.brayner@cnen.gov.br

abel.rodriguez@ufpe.br

ABSTRACT

Wax deposition along the extensive oilfield pipelines is a problem that affects the flow assurance. To solve it, one must monitor the wax formation in its initial stage. In this light, nuclear techniques are an effective alternative solution, as they can detect characteristics of materials or substances in an indirect and non-invasive manner. The present work shows a computational model using the MCNP6 (*Monte Carlo N-Particle 6*) code and the gamma radiation transmission profiling technique to detect different wax thickness. This fact is directly related to the attenuation of the gamma radiation beam when crossing the wax thicknesses.

Keywords: **wax deposition, gamma radiation, Monte Carlo method.**

ISSN: 2319-0612
DOI: https://doi.org/10.15392/2319-0612.2023.2193
Submitted: 2022-12-26
Accepted: 2023-06-26

1. INTRODUCTION

Oil production in deep and ultra-deep waters has its own characteristic challenges to flow assurance, among which is wax deposition along the extensive production pipelines.

This deposition occurs because waxes of high molecular weight, and thus with a higher number of carbons, are present in the solid phase under normal temperature and pressure conditions. However, in oil reservoirs, such as those in pre-salt fields, waxes are initially solubilized in the liquid phase of the oil in a state of equilibrium [1]. In this condition, oil temperatures range from 70ºC to 150ºC, with pressure greater than 2,000 psi, behaving as a Newtonian fluid [2]. But this condition changes when the oil is extracted from the reservoir or oil well, given that, when it is extracted and enters the production line, the oil starts to cool along the pipeline due to a radial temperature gradient, which causes heat loss to the external environment. This problem occurs more frequently in offshore environments, where most of the Brazilian reservoirs are located and where the ocean temperature, at high depths, is around 5°C. As the oil is cooled and reaches the Wax Appearance Temperature (WAT), the process of precipitation and subsequent wax deposition starts on the internal walls of the pipeline [3]. This deposition process is represented in Figure 1.

Figure 1: *Wax deposition process on the inner wall of the pipeline*

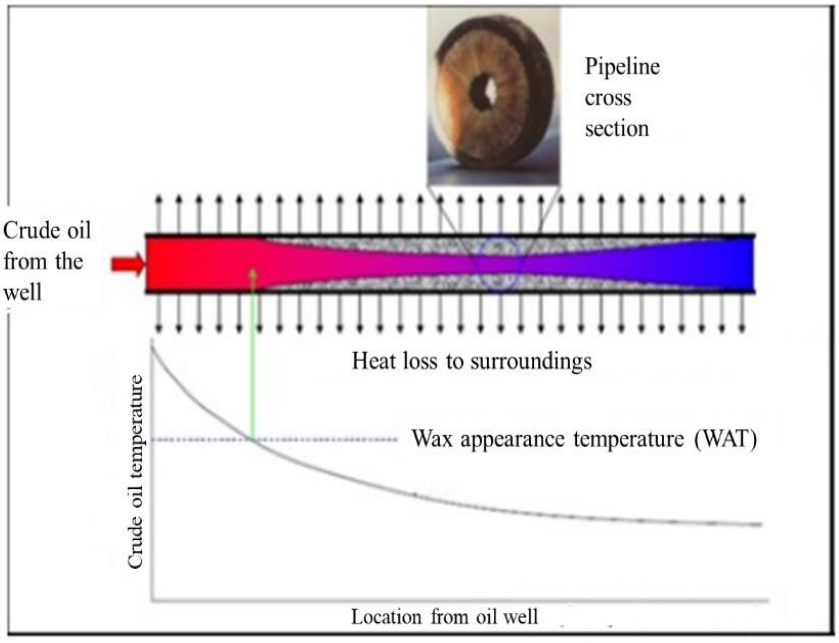

Source: Adapted from [4].

As can be seen in Figure 1, the wax deposition rate is initially high, but it decreases as more wax is deposited on the duct surface. This is because when the wax thickness increases, it begins to act as a thermal insulator, reducing the temperature gradient [4].

In addition to the concentration of high molecular weight wax solubilized in the oil and the temperature gradient, other factors that influence wax deposition are oil pressure, amount of free gas in the oil flow, flow velocity, and pipeline surface properties [5].

Wax deposition causes an increase in pipeline roughness, which leads to increased friction losses, restricted production, and in more extreme cases, losses in the production line due to total pipeline plugging [6-7], as shown in Figure 2.

Figure 2: *Pipelines clogged by wax deposition.*

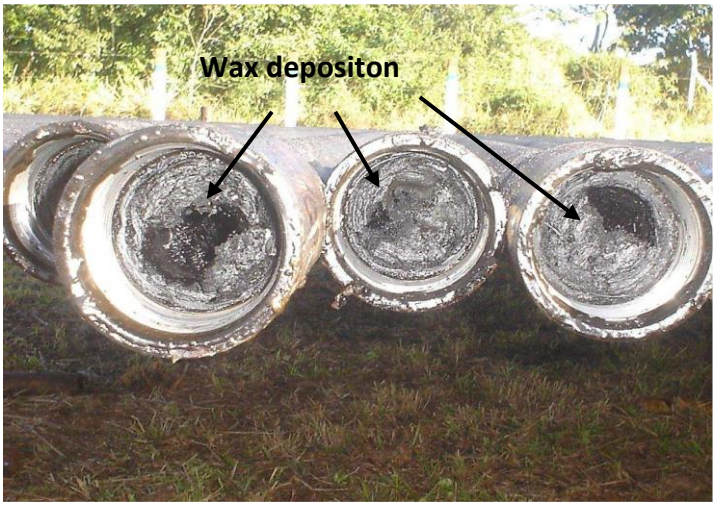

Source: [8]

The problem of wax deposition and formation occurs in the various stages of oil handling, during production, transport, and refining. Moreover, in Brazil, Petrobras, internationally recognized as the holder of technology in exploration and production in deepwater and ultra-deepwater, often faces this problem in its submarine lines [1]. The problem is also a major cause of economic losses for oil and gas companies (such as Petrobras), which can reach millions of dollars per year worldwide through the enormous cost of prevention and remediation, reduced or delayed production, well closures, replacement and/or abandonment of pipelines, equipment failure, extra power requirements, and increased manpower needs [9].

Traditionally, oil companies have been forced to remove wax deposits from pipelines using mechanical, chemical, and thermal methods, where in many cases a combination of two or more of these methods are employed [10]. However, such methods have always had problems and limitations, where research continues to be done to find the most efficient, economical, and safe methods to remove wax deposits and blockages [11].

Earlier identification of hydrocarbon deposits within oil pipelines during operation will reduce maintenance costs by minimizing both unnecessary pipe replacements and plant shutdown for inspection [12]. As oil and gas production moves into deeper, colder waters, it becomes increasingly imperative to properly identify wax precipitation conditions and predict wax deposition rates to optimize the design and operation of subsea multiphase production systems [9]. Timely location, measurement, and removal of wax deposits saves money for oil extraction plant operation [13].

In view of the above, the solution to solve the problem of wax deposition in pipelines requires the development of methods and application of techniques to monitor the wax formation in its initial stage. Many studies, methods, and techniques are found in the literature for this purpose, however most of them require direct contact with the pipeline structure to predict or detect wax deposition. In view of this, nuclear techniques present themselves as an alternative because it can detect characteristics of materials or substances in an indirect and non-invasive manner [14-17].

However, there are few studies in the literature specifically focused on wax monitoring using gamma radiation [5,18, 19]. Therefore, this paper aims to develop a computational model using the MCNP6 (*Monte Carlo N-particle 6*) code for wax detection in deepwater pipelines together with the gamma radiation transmission profiling technique.

2. MATERIALS AND METHODS

2.1. Gamma radiation transmission

The penetrating power of gamma radiation into matter depends on the interaction probability or cross section for each type of event (photoelectric absorption, Compton scattering, pair production and/or Rayleigh scattering) that can absorb or scatter the incident radiation and its penetrability is much higher than that of alpha and beta particles [20].

The attenuation of a narrow, parallel beam of monoenergetic gamma photons penetrating a thin plate of homogeneous material is known to follow the Lambert-Beer exponential decay law [21]:

$$I = I_0 e^{\mu x} \tag{1}$$

Where I_0 is the incident or initial intensity, x is the thickness of the medium, I is the intensity of the remaining beam, and μ is the linear attenuation coefficient, which expresses the interaction probability of the photon per unit path length in the medium. This coefficient is strongly dependent on the radiation energy, density, and atomic number of the medium, and is the sum of the contributions of several independent interaction mechanisms: photoelectric absorption, Compton scattering, pair production and Rayleigh scattering.

In the case of a material composed of n layers of different elements and thicknesses, the intensity I of the transmitted beam is given by [20]:

$$I = I_0 e^{-\sum_{i=1}^{n} \mu_i x_i} \tag{2}$$

From Equation 1, the number of photons transmitted by a medium I is given in terms of the number of photons without the medium I_0 as [21]:

$$\frac{I}{I_0} = e^{\mu x} \tag{3}$$

Figure 3 shows an incident beam of monoenergetic photons from a collimated source hitting a detector after passing through a material of varying thicknesses.

Figure 3: *Representation of the exponential gamma radiation transmission curve for monoenergetic beam*

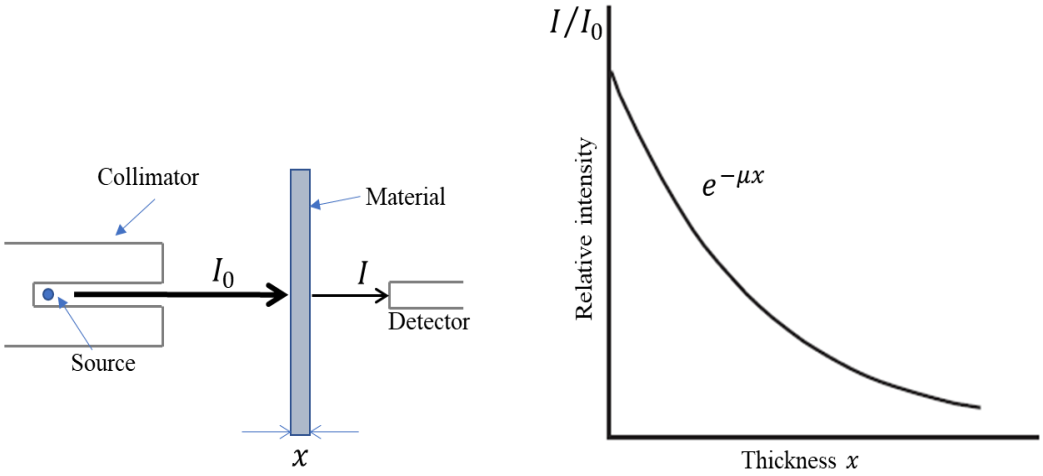

Source: Adapted from [22].

According to Equation 3 the result should be an exponential curve of the thickness x versus the relative intensity $\frac{I}{I_0}$. However, the narrow beam configuration is referred to as good geometry and is rarely achieved in a realistic measurement system, as a portion of the interacting photons outside the beam defined by the source/detector geometry is scattered toward the detector aperture and contributes to the measured intensity. Whenever a significant fraction of the scattered or secondary photons reaches the detector, the arrangement is called a broad beam or bad geometry [21]. Because of this, an accumulation factor is introduced $B(\mu, x)$, in the following the equation:

$$\frac{I}{I_0} = B(\mu, x)e^{-\mu x} \tag{4}$$

The factor $B(\mu, x)$ depends on the linear attenuation coefficient and its composition, and the thickness and geometry of the material in which the scattering is generated, which can be the shielding of the source and detector, the measurement object itself, or even the encapsulation of the source and detector. When there is a good geometry of the experiment, this factor is equal to 1, but otherwise it cannot be calculated analytically, and must be determined from experiments, simulations, or models [21].

2.2. Gamma Radiation Transmission Profiling Technique

This technique consists of moving a source-detector system along the cross section of a duct for the gamma radiation beam to scan through a pre-set step (Figure 4, left side). For each position the photon count or relative intensity (I/I_o) is recorded. With all counts a profile graph is drawn up (Figure 4, right side).

Figure 4: *Gamma radiation transmission profiling technique*

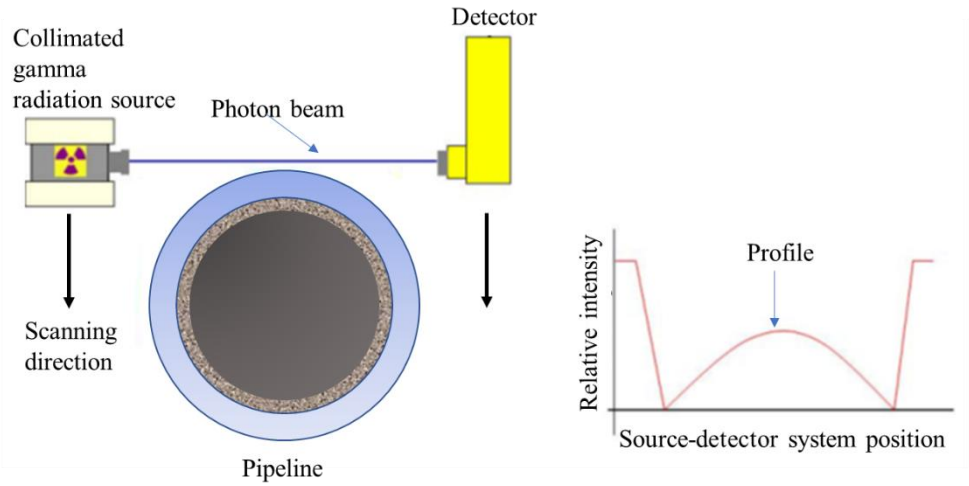

Source: Adapted from [15].

According to the graph in Figure 4, the relative intensity varies according to the position of the radiation beam, i.e., the position of the source-detector system. This is because, when passing through different materials, the beam will be attenuated according to the density and thickness of each material, as explained in section 2.1.

Mccaw et al. [23] seems to have been the first to publish on the use of this technique in industry, when he used it to inspect heavy water plant towers of 8.5 m diameter and 8.9 cm wall thickness [21]. More recent work researched on the use of the technique can be found in the references [14-17, 24].

2.3. Monte Carlo Method and the MCNP6

Due to its random nature, the transport of radiation through materials is a complex process that is generally impossible to solve analytically. Monte Carlo (MC) methods simulate the random

trajectories of individual particles (photons) using computer-generated pseudo-random numbers to sample the probability distributions that govern the physical processes involved. By simulating a large number of histories, information can be obtained about average values of macroscopic quantities, such as energy deposition in predefined volumes in a radiation detector. In addition, since the histories of individual particles are followed, the method can be used to obtain information about the statistical fluctuations of particular types of events. The availability of computers with high processing power makes MC simulation an attractive alternative for experimental testing [21].

There are a variety of MC simulation codes available, but all of them have four main components in common: The geometry definition interface, the cross-sectional data for all the processes considered in the simulation, the algorithms used for radiation transport, and finally the interface to analyze the information obtained during the simulation [21].

The MCNP particle radiation transport code, which stands for *Monte Carlo N Particle*, is a general-purpose three-dimensional simulation tool that transports 37 different types of particles for criticality, shielding, dosimetry, detector response, and many other applications [26].

MCNP6 version 1.0, released in May 2013, could be simply and accurately described as the combination of the MCNP5 and MCNPX features, but it is much more than the sum of these two computer codes. MCNP6 is the result of six years of effort by the MCNP5 and MCNPX code development teams and incorporates several new possibilities and features for computational simulation not found in previous versions [27].

According to the MCNP6 manual, to perform a simulation, an input file containing all the input information to describe the problem must be prepared, namely [26]:

Cell cards: where the geometry data of the problem is described, using combinations of predefined geometric shapes, such as planes, spheres, cylinders, etc., described on the *surface card* (described below), using combinations through Boolean operators such as intersections and unions. This card must also contain the materials whose compositions are on the *data cards (described later*) and their respective densities. Another piece of data that can and must be included with the *cell card* is the importance of each cell defined in the *imp card*.

Surface card: where the geometric shapes to be used in the problem geometry are selected. For this, mnemonic characters are used, indicating the type of surface and the coefficients of the equation of the selected surface.

Data cards: where the physical data of the problem is described, composed of the following cards:

Mode card: defines the type (or types) of radiation used in the problem, through the letters P (Photons), E (Electrons), and N (Neutrons).

Material card: where the types of materials and their respective atomic compositions are defined.

Source card: where type, energy, position, direction, and particle of the radiation source are defined.

Tally card: where you define the tally type, i.e., what you want to write to the output data at the end of a run.

And finally, the problem boundary, or *cutsoffs*, where the user-imposed limits for completing the problem execution, such as number of stories (NPS command), time, energy, etc., are presented.

2.4.Methodology

To achieve the objective of this work, a computational model will be used to simulate the transport of monoenergetic gamma photons using the MCNP6 version 1.0 code and the gamma radiation transmission profiling technique. Figure 5 represents the scheme of the model.

Figure 5: *Schematic representation of the computational model for simulation*

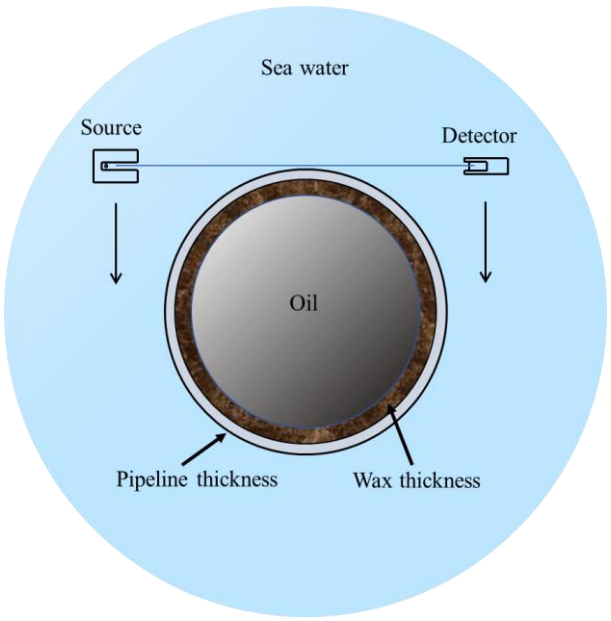

In the proposed model, the seawater consists of saltwater with a 4% mass fraction of sodium chloride (NaCl), the same as suggested by Beserra [15] and Salgado [28] in their simulations with MCNP. According to Gouveia [29], for rigid pipelines installed at depths above 1,000 meters, the steel used is API grade X-60 or X-65, with a composition of iron equal to or greater than 95%, as shown in the manufacturer's catalog Tuper [30]. As shown by Beserra [15], due to this high percentage of iron in the steel, for simulation purposes in the MCNP, it is feasible to adopt only this element as the steel composition. The choice of oil is in accordance with Thomas [31], according to which the oils obtained from different petroleum reservoirs have different characteristics, however, they all produce similar elemental analyses. In view of this, Texas crude oil will be used, considering the publication of the chemical composition data of this oil [32]. Waxes are alkanes whose general formula is C_nH_{2n+2} [31]. Dobbs [33] reports that the hard crystalline waxes have 25 to 50 or more carbons in the chain. In view of this, the wax $C_{25}H_{52}$ contained in reference [32] will be considered.

To validate the computational model to be used, the experimental data reported by Oliveira et al. [17] will be used. Among the four graphs presented by the authors, one identified the presence of a barium oxide ($BaSO_4$) scale on the internal walls of an 18" (450 mm) diameter and 40 mm thick duct used in the petroleum industry. About the experiment, the authors reported that the profiling in the duct was performed in 5 mm steps, with no overlap between inspection points, and that the detector recorded the radiation intensity point by point, according to the thickness penetrated in the duct chord. With that, they obtained an intensity profile related to the position of the scanning system. For each point, the acquisition time was 60 s. The results showed that the duct was empty (or filled with air) and contained a 21 mm thickness of $BaSO_4$ scale. However, the authors did not mention the resulting uncertainty at each step of the profile. Figure 6 shows this plot with only the experimental data, which have been extracted by the WebPlotDigitizer software [34].

Figure 6: *Profiling of a pipeline with $BaSO_4$ scale*

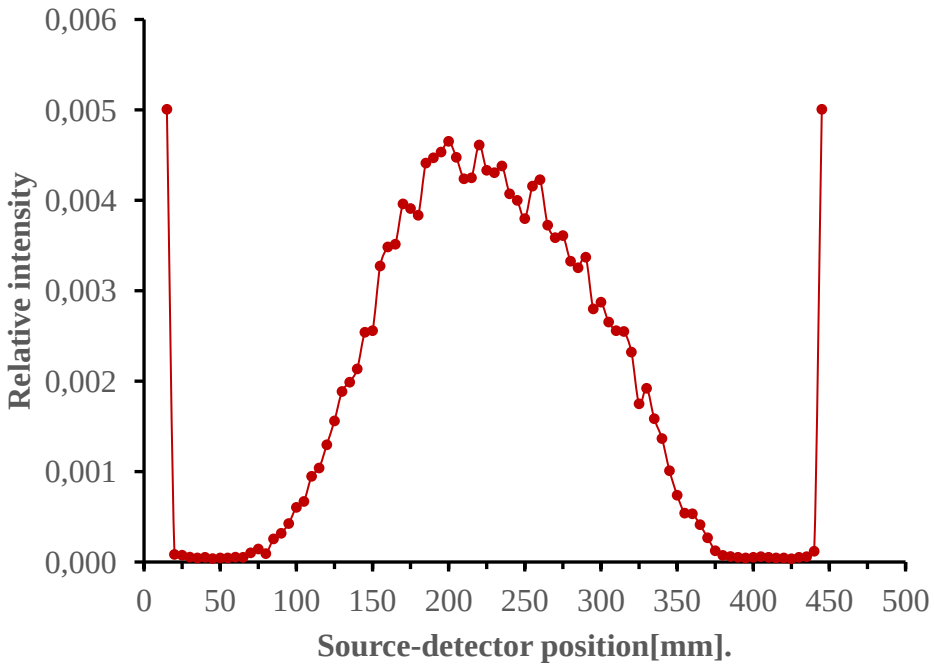

Source: Adapted from [17].

These data will be compared with data simulated in MCNP6. In this case, both geometric representations and material properties reported by the authors will be used.

The steps for the model validation are shown in Figure 7.

Figure 7: *Flowchart for validating the computational model.*

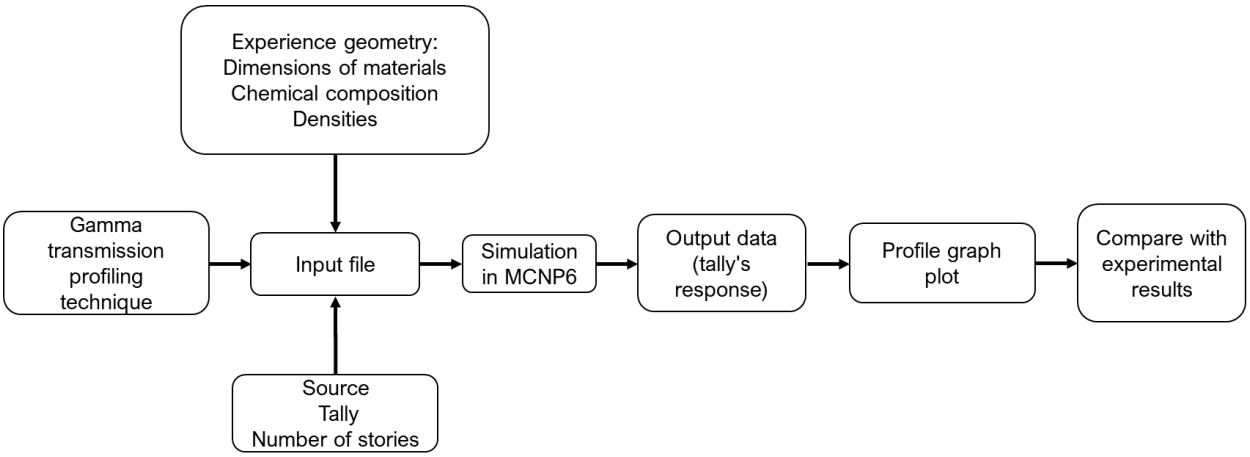

Data on geometric dimensions, densities, chemical compositions of all materials involved, source and detector will be inserted according to information from Oliveira et al. [17]. A 662 keV pencil beam source - corresponding to the radioisotope ^{137}Cs - and a 5 mm diameter cylindrical shape representing the detector, positioned on the other side of the duct, diametrically opposite to the source, will be used. For this case, the tally used will be F1 (which provides the relative intensity of photons arriving at the detector) and a number of 10^7 photon histories, which is the limit that the source provides to finish the simulation run. A step of 5 mm between each source-detector position and a fixed distance between source and detector of 460 mm will be established. For the application of the gamma radiation transmission profiling technique, 91 input files (one for each source-detector position) will be prepared and then run in the MCNP6 code to provide 91 output files, providing their corresponding gamma radiation relative intensity value (tally F1), as well as the related error.

Once validated, the computational model will be used to identify the presence of wax in the inner walls of a pipeline located in deep water from the gamma transmission profiles for different thicknesses. For this purpose, a 355.6 mm (14") diameter and 35.7 mm thick pipeline will be used, taken from reference [29], where profiling will be done in 7.1 mm steps.

The steps of the computational model for wax detection are shown in Figure 8.

Figure 8: *Flowchart of the computational model for detecting wax in a pipeline.*

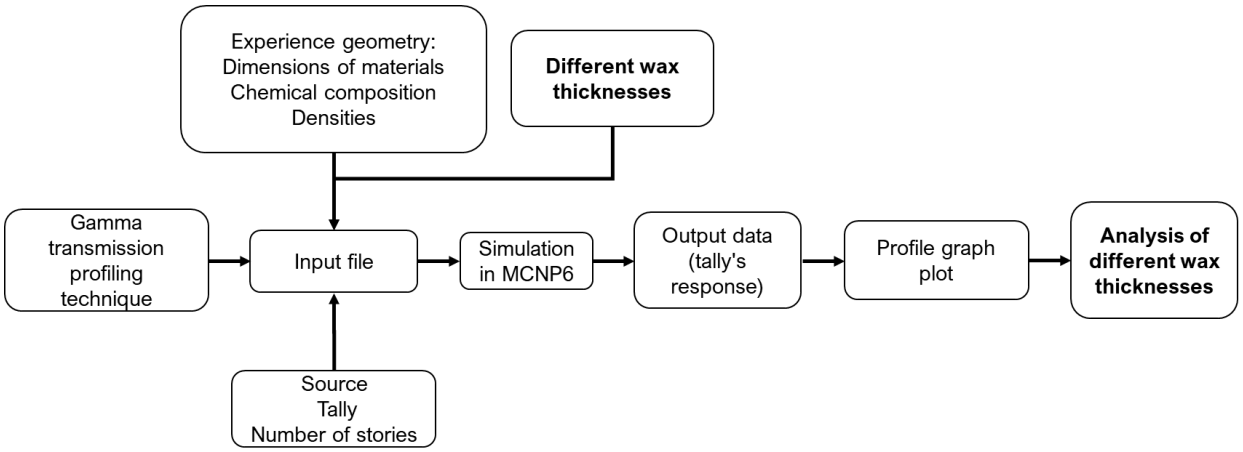

Following the flowchart presented in Figure 8, the input file will be prepared according to the MCNP6 user manual [25], with geometry data, materials and densities of the elements presented in Figure 5. The remaining data for the preparation of the input file will be as follows:

- 662 keV pencil beam source, which corresponds to the energy of the radioisotope ^{137}Cs.
- P-mode set for photon transport.
- Tally F1 to provide the relative intensity of photons arriving at the detector.
- NPS equal to $5x10^7$ histories of photons.

The detector is represented by a cylinder with a diameter of 5 mm, because in simulation terms what matters is the number of photons (or relative intensity) defined by tally F1 that crosses a flat surface, in this case the cylinder face.

For the execution of the profiling technique, 25 input files will be prepared, one for each position along the cross section of the pipeline up to half of it, since the other half is symmetrical considering the concentric distribution of the wax layer. These files will be run in MCNP6 to provide 25 output files. From each of these files the tally result was extracted and a plot of source-detector position versus relative intensity was plotted, as per Figure 10. To highlight the wax detection, profiles will be plotted, with the first considering the pipeline without paraffin and the others with thicknesses of 5, 10, 20, 30 and 70% in relation to the internal radius. With this, the total number of files produced will be 150, both inlet and outlet.

3. RESULTS AND DISCUSSION

3.1. Validation of the computational model

Figure 9 shows the curves with the experimental data from Oliveira et al. [17] and those simulation results in MCNP6.

Figure 9: *Comparison between experimental and simulated data in MCNP6*

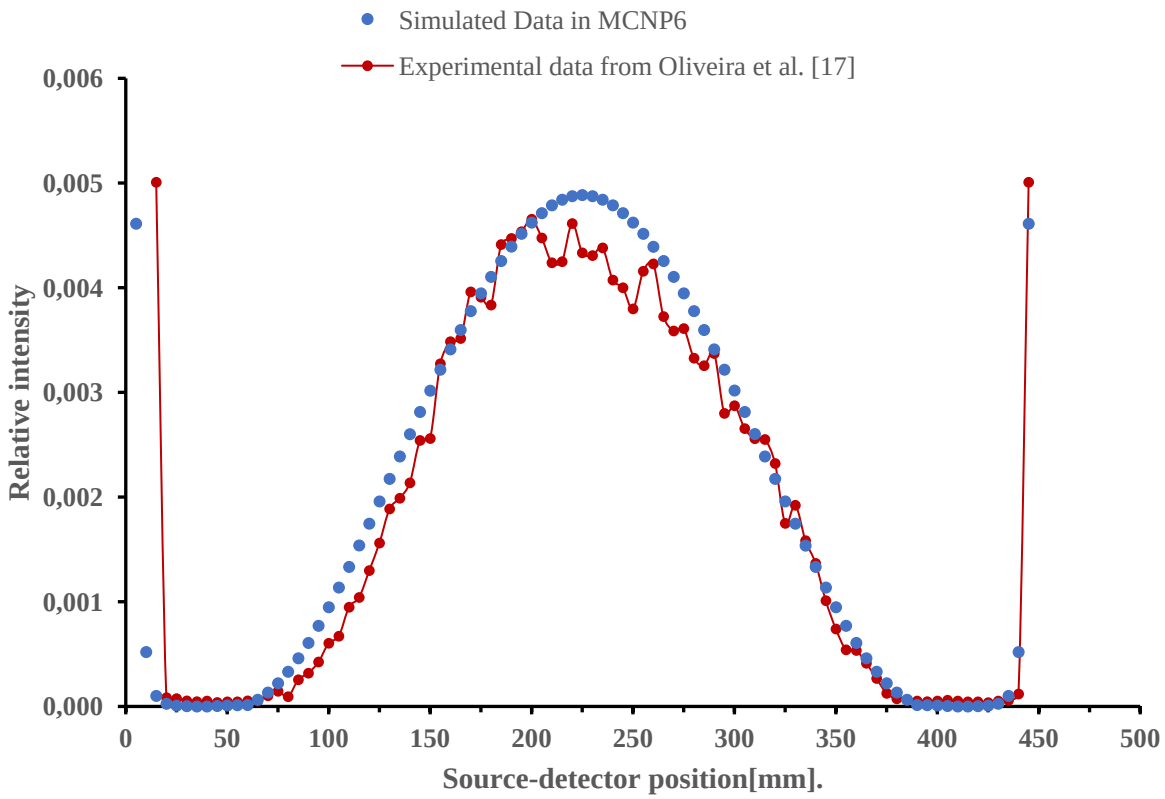

Figure 9 shows that there is a similarity between the graphs. However, the authors did not give information about the degree of uncertainty of their measurements, which makes it difficult to compare the experimental and simulated data in this work. Beserra [15], making use of experimental data from Marinho et al. [14] - who also used the gamma transmission profiling technique to detect $BaSO_4$ scale in oil pipelines under the same conditions presented here - reports that the differences between the experimental and simulated data for an air-filled pipeline arise from the tendency of scale to eccentric deposition, coupled with the lack of material.

It should be taken into consideration that the differences also occur due to the simplification of the computational model used to carry out the simulation, mainly in relation to scale and source. About the scale, the composition of $BaSO_4$ inserted in the MCNP6 besides not predicting the absence of material from the experimental sample, also does not predict other factors existing in the environment where the experiment was performed. As for the source, in the simulations of this study the pencil beam type was used, while in the experiment of Oliveira et al. (2015), the collimated type. As analyzed by Beserra [15], the interaction of photons from a collimated source is faster on the

pipeline wall than the photons from a pencil beam source and this fact also contributes to the differences between the simulated and experimental data.

3.2. Wax detection

Figure 10 shows the simulated profiles in the computational model, according to the flowchart in Figure 8.

Figure 10: *Profiling the pipeline with different wax thicknesses.*

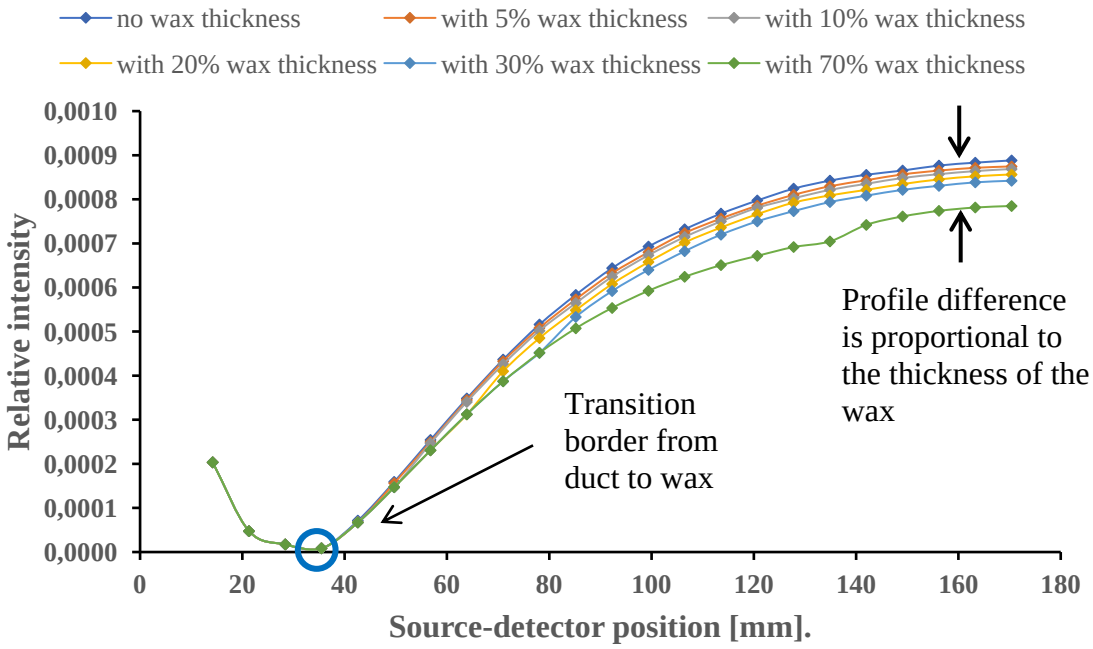

It can be seen in Figure 10 that after the gamma beam crosses the boundary between the inner edge of the duct and the wax (blue highlight at the bottom of the Figure), the transmission profiles differ at each step (highlighted at the top of the Figure), being directly proportional to the wax thickness. The difference is caused by the greater attenuation of gamma radiation with the addition of wax on the inner wall of the duct, so that it is possible to detect its presence and even predict its thickness.

Adopting the wax-free pipeline condition as the reference and comparing it with any other condition of the pipeline containing wax, this difference becomes more evident. Figure 11 shows, for example, a comparison between 30% wax and the reference, highlighting the position of the profile where the transition from wax to oil occurs. This transition is also referred to in the literature as a

jump [5]. This result points out that the sensibility of the model is less to the little wax thicknesses and higher with the increase the wax thicknesses. This is a main its limitation of the proposed model.

Figure 11: *Difference between the pipeline without wax and with 30% wax*

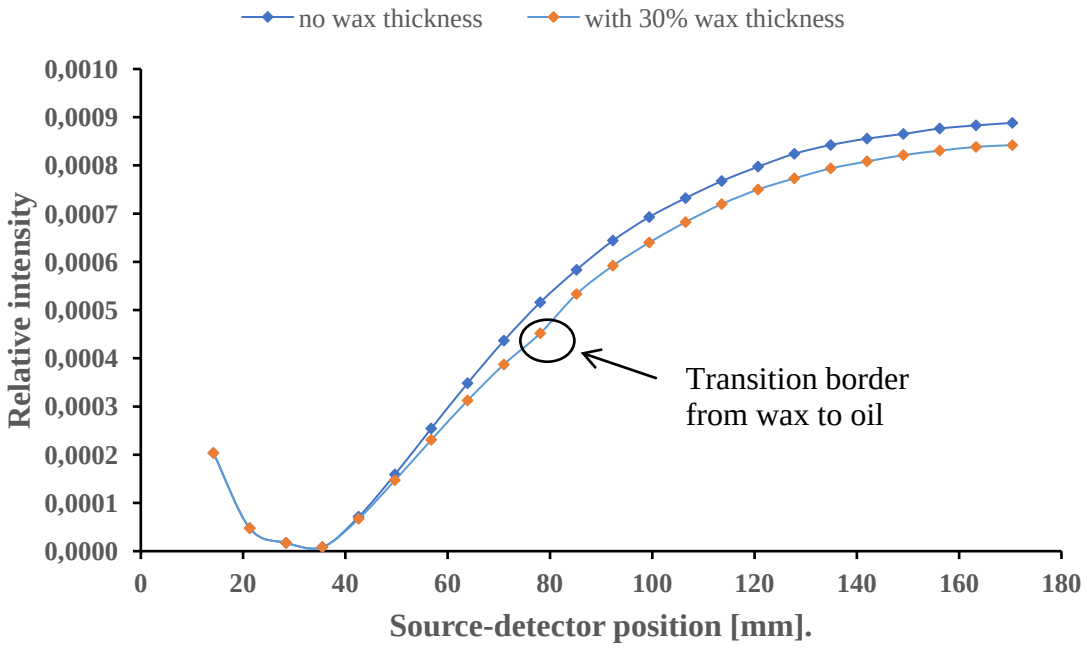

4. CONCLUSIONS

Detecting wax deposition on the internal walls of pipelines in their early stages avoids unscheduled downtime and even blockage of oil extraction lines. Nuclear techniques are an effective alternative solution, given that they can indirectly and non-invasively detect the presence of material inside the pipeline.

The results of this work show that the computational model based on the gamma radiation transmission profiling technique can detect different wax thicknesses. This fact is due to the higher attenuation of the radiation beam when crossing the wax layer. The difference between the transmission profiles is proportional to the thickness of its layer. From that, it is possible to estimate the thickness of the wax.

A computational model based on the gamma radiation transmission profiling technique was elaborated and validated partially by a comparison with experimental data from the literature. The differences between simulated results and experimental data are due to some simplifications of the

proposed model. The main simplification is because the analyzed layer of $BaSO_4$ was considered as a homogeneous and concentric layer. Did not consider the wet of air was another important simplification. This environmental factor and the irregularities of the sample itself contribute to the difference between the result and the experimental data.

REFERENCES

[1] BORDALO, S. N.; OLIVEIRA, R. Biphasic oil-water flow with wax precipitation in subsea oil production pipelines. **4º PDPETRO**, p. 12, 2007.

[2] MATOS, S. F.; ALTOÉ, L. Analysis of deepwater oil flow assurance in relation to wax deposition. **Latin American Journal of Energy Research**, v. 6, p. 12-31, 2020.

[3] PORTO, T. R. N.; LIMA, A. G. B. De. Transient flow of waxy oil in a circular section pipeline: modeling and simulation. Holos, v. 1, p. 155, 2017.

[4] THEYAB, M. A. Wax deposition process: mechanisms, affecting factors and mitigation methods. **Open Access Journal of Science**, v. 2, 2018.

[5] KOPTEVA, A.; KOPTEV, V.; MALAREV, V.; USHKOVA, T. Development of a system for automated control of oil transportation in the Arctic region to prevent the formation of wax deposits in pipelines. **E3S Web of Conferences**, v. 140, 2019.

[6] LIU, L.J.; SCOTT, S.L. A new method to locate partial blockages in subsea flowlines. **Society of Petroleum Engineers Inc**, 2001.

[7] CRUZ, D. E. **Study of paraffin deposition in multiphase flow in pipelines**. Rio de Janeiro: Pontifical Catholic University of Rio de Janeiro, 2011.

[8] XAVIER, F. M.; CAVALCANTI, V. D.; MANZELA, A. A. Challenges of flow assurance in the exploration of pre-salt fields. **Revista de engenharias da faculdade salesiana**, v. 3, p. 33-44, 2016.

[9] CHEN, X. T.; BUTLER, M.; VOLK, M. Techniques for measuring wax thickness during single and multiphase flow. **Society of Petroleum Engineers Inc**, 1997.

[10] WOO, G. T.; GARBIS, S. J; GRAY, T. C. Long-term control of wax deposition. **Society of Petroleum Engineers of AIME**, 1984.

[11] AIYEJINA, A.; CHAKRABARTI, D. P; PILGRIM, A; SASTRY, M. K. S. Wax formation in oil pipelines: A critical review. **International Journal of Multiphase Flow**, v. 37, p. 671-694, 2011.

[12] MAJID, S. A.; MELAIBARI, A; MALKI, B. Hydrocarbon scale deposits measurements by neutron moderation and capture gamma methods. **Nuclear Instruments and Methods in Physics Research B**, v. 119, p. 433-437, 1996.

[13] MAJID, S. A. Determination of wax deposition and corrosion in pipelines by neutron back diffusion collimation and neutron capture gamma rays. **Applied Radiation and Isotopes**, v. 74, p. 102-108, 2013.

[14] MARINHO, C. A.; COSTA, R. D.; SANTOS, E.; COSTA, A. K.; OLIVEIRA, D.; LOPES, R. Monitoring and quantification of scale using radiographic methods: scientific supplement. **CONAEND&IEV2008**, 2008.

[15] BESERRA, M. T. F. **Evaluation of scale thickness in oil extraction pipelines**. Rio de Janeiro: Instituto de Radioproteção e Dosimetria, 2012.

[16] SOARES, M. **Scale detection system in oil transportation pipelines by gamma transmission technique**. Rio de Janeiro: Federal University of Rio de Janeiro, 2014.

[17] OLIVEIRA, D. F.; NASCIMENTO, J. R.; MARINHO, C. A.; LOPES, R. T. Gamma transmission system for detection of scale in oil exploration pipelines, **Nuclear Instruments and Methods in Physics Research A**., 2015.

[18] LOPES, R. T.; VALENTE, C. M.; DE JESUS, E. F. O.; CAMERINI, C. S. Detection of paraffin deposition inside a draining tubulation by the Compton Scattering Technique. **Applied Radiation and Isotopes**, 1997. v. 48, n. 10–12, p. 1443–1450.

[19] KOPTEV, V. Y.; KOPTEVA, A.V. Improving paraffin deposits detection methodology for better ecological safety during hydrocarbon transportation. **International Journal of Applied Engineering Research**, v. 12, p. 618-621, 2017

[20] TAUHATA, L.; SALATI, I.; PRINZIO, R. D.; PRINZIO, A. R. D. **Radioprotection and Dosimetry: Fundamentals**. 10ª ed. Rio de Janeiro: Comissão Nacional de Energia Nuclear, 2014.

[21] JOHANSEN, G. A.; JACKSON, P. **Radioisotope Gauges for Industrial Process Measurements**. 1ª ed. Chichester: John Wiley & Sons Ltd, 2004.

[22] KNOLL, G. F. **Radiation Detection and Measurement**. 4ª ed. Michigan: John Wiley & Sons Inc, 2010.

[23] MCCAW, D. D.; HULBERT, V. G.; SMITH, A. E. Gamma scanning of large sieve tray towers. **Atomic Energy of Canada Limited**, 1975.

[24] CARNEIRO JUNIOR, C. **Development of an inspection system based on gamma transmission for application in flexible ducts and industrial columns**. Rio de Janeiro: Universidade Federal do Rio de Janeiro, 2005.

[25] KOPTEV, V. Y.; KOPTEVA, A.V. Improving wax deposits detection methodology for better ecological safety during hydrocarbon transportation. **International Journal of Applied Engineering Research**, v. 12, p. 618-621, 2017.

[26] LOS ALAMOS NATIONAL LABORATORY. **MCNP6.1/MCNP5/MCNPX User manual.** Los Alamos: 2013.

[27] GOORLEY, J. T.; JAMES, M. R.; BOOTH, T. E.; BROWN, F. B.; BULL, J. S.; COX, L. J.; DURKEE, J. W. J.; ELSON, J. S.; FENSIN, MICHAEL LORNE FORSTER, ROBERT A. III HENDRICKS, J. S.; HUGHES, H. G. I.; JOHNS, R. C.; KI, A. J. **Initial MCNP6 release overview - MCNP6 version 1.0**. Los Alamos: 2013. p. 0-42.

[28] SALGADO, C. M. **Identification of Flow Regimes and Prediction of Volume Fractions in Multiphase Systems Using Nuclear Technique and Artificial Neural Network**. Federal University of Rio de Janeiro, 2010

[29] GOUVEIA, J. C. C. **Critical engineering analysis for rigid pipes submitted to large deformations**. Rio de Janeiro: Fluminense Federal University, 2010.

[30] TUPER. **API Pipes**. Available at: < https://www.tuper.com.br/wp-content/uploads/2019/10/Catalogo-de-Tubos-API-Tuper.pdf>. Accessed: September 25, 2021.

[31] THOMAS, J. E. **Fundamentals of petroleum engineering**. Rio de Janeiro: Editora Inteligência, 2001.

[32] MCCONN, R.; GESH, C.; PAGH, R.; RUCKER; WILLIAMS, R. **Compendium of material composition data for radiation transport modeling**. Washington, 2011.

[33] DOBBS, J. B. A unique method of wax control in production operations. **Society of Petroleum Engineers Inc**, 1999

[34] AUTOMERIS. **WebPlotDigitizer**. Available at: https://automeris.io/WebPlotDigitizer/. Accessed on: July 06, 2022.